ON TENTH-ORDER CENTRAL SPATIAL SCHEMES

Björn Sjögreen*
Center for Applied Scientific Computing,
Lawrence Livermore National Laboratory
Livermore, CA 94551, USA
sjogreen2@llnl.gov

H.C.Yee
NASA Ames Research Center,
Moffett Field, CA 94035, USA
hmcyee@mail.arc.nasa.gov

ABSTRACT

This paper explores the performance of the tenth-order central spatial scheme and derives the accompanying energy-norm stable summation-by-parts (SBP) numerical boundary operators for problems with non-periodic boundaries. The objective is to employ the resulting tenth-order spatial differencing with the stable SBP boundary operators as a base scheme in the framework of adaptive numerical dissipation control in high order multistep filter schemes of Yee et al. (1999), Yee and Sjögreen (2002, 2005, 2006, 2007), and Sjögreen and Yee (2004). These schemes were designed for multiscale turbulence flows including strong shock waves and combustion.

INTRODUCTION

The accuracy and stability of the overall high order central difference operators employing the traditional ways of implementing numerical boundary conditions by reducing the orders of the central scheme near the non-periodic boundary can be greatly compromised. In the 80's and 90's major effort was placed on the development of high order shock-capturing schemes and high order compact spatial schemes. Traditional high order central schemes were considered neither stable nor robust enough to be used in a more practical setting. In the work of Kriess and Scherer (1974, 1977), Strand (1994), Olsson (1995), Mattsson (2003), Svärd (2004) and references cited therein, high order finite difference operators containing special numerical boundary conditions with summation-by-parts (SBP) stable energy estimates were derived for the first derivative approximations for centered difference operator (for the interior grid points) of order up to eight. The use of standard central spatial schemes thus regained its momentum in the mid and late 90's. These SBP central schemes up to order eight have been used with much success as the spatial base scheme in the adaptive numerical dissipation control high order multistep filter schemes of Yee and Sjögreen (1999, 2002, 2005, 2006, 2007) and Sjögreen and Yee (2002, 2003, 2004). Their test examples concentrated mainly on SBP sixth-order central spatial base schemes. Improved accuracy over standard high order shock-capturing schemes was obtained for multiscale shock/turbulence interactions.

In this work, the tenth-order central spatial differencing with stable SBP boundary operators is derived with numerical examples. The next section illustrates the performance of the tenth-order scheme for problems with periodic physical boundaries. The SBP boundary operators for the tenth-order centered differencing are derived with a 1-D shock/turbulence interaction example in the subsequent sections. 2-D and 3-D examples are in progress and will be reported in a forthcoming paper. From here on, the use of the phrase, e.g., "SBP tenth-order central schemes" means the use of the tenth-order centered differencing interior scheme (for the interior grid points) with the accompanying stable SBP boundary operators of orders that are usually much lower than the interior scheme.

TEST CASES WITH PERIODIC BOUNDARY CONDITIONS

This section shows the performance of the tenth-order spatial scheme for several test cases with periodic boundary conditions. Note that in this case, SBP boundary operators are not needed.

The seven-point, sixth-order accurate centered difference operator (D06) with an eighth-order numerical dissipation (AD8) is denoted by D06AD8. The eleven-point, tenth-order accurate centered difference operator (D10) with twelfth-order numerical dissipation (AD12) is denoted by D10AD12. Similarly, D08AD10 denotes the eighth-order centered difference operator (D08) with tenth-order numerical dissipation (AD10). These operators are used for the spatial derivatives in the Euler equations. The classical fourth-order accurate Runge-Kutta method is used for the time integration. In all of the examples, different time step sizes that are below the CFL limit were used. However, their results indicate no significant difference in the accuracy, indicating that the error of the spatial discretization dominates the temporal error.

The first example is the same isentropic vortex convection problem considered in Yee et al. (1999) and Sjögreen and Yee (2002). The computational domain is $[0, 18] \times [0, 18]$.

*Work performed under the auspices of the U.S. Department of Energy by University of California Lawrence Livermore National Laboratory under contract No. W-7405-Eng-48. UCRL-CONF-230974

The initial data is

$$\rho(0,x,y) = \left(1 - \frac{\beta^2(\gamma-1)}{8\gamma\pi^2} e^{1-r^2}\right)^{\frac{1}{\gamma-1}} \tag{1}$$

$$u(0,x,y) = u_\infty - \frac{\beta}{2\pi}(y-y_0)e^{(1-r^2)/2} \tag{2}$$

$$v(0,x,y) = v_\infty + \frac{\beta}{2\pi}(x-x_0)e^{(1-r^2)/2} \tag{3}$$

$$p(0,x,y) = \rho(0,x,y)^\gamma \tag{4}$$

where ρ is the density, u is the velocity in the x-direction, v is the velocity in the y-direction, and p is the pressure. γ is the ratio of specific heats. Here, $\gamma = 1.4$, $\beta = 5$, $u_\infty = 1$, and $v_\infty = 0$. $r^2 = (x-x_0)^2+(y-y_0)^2$, where the initial center of the vortex is $(x_0, y_0) = (9, 9)$. The boundary conditions are periodic in both directions. The exact solution consists of a translation of the initial data with the free stream velocity.

Figure 1 displays the L^2-norm error in the density after one computational domain period of time integration with D06AD8 (solid line) and D10AD12 (dashed line) for four uniform grids with spacings $h = 0.5$, 0.25, 0.125, and 0.0625. The dissipation coefficient for AD8 is 0.0016 and for AD12 is 0.0001. We infer from Fig. 1 that the error of the tenth-order method is always smaller than the error of the sixth-order method, but that the errors of both methods converge slower than the formal order of accuracy for the first two refinements. At the last refinement, the results are closer to the expected convergence rate. The error of the sixth-order method decreases by a factor 69, when we refine from $h = 0.125$ to $h = 0.0625$. The corresponding decrease of the error in the tenth-order method is a factor 692. The reduction of the error between the coarsest grids is slow because the computation is under resolved for h larger than 0.25. The highest significant frequencies are not resolved with any points per wavelength; points per wavelength results become meaningless. Computations without the added numerical dissipation are also stable. However, spurious oscillations due to the nonlinear effect of the governing equations prevent the convection of the vortex from advancing to a higher number of periods. See Sjögreen and Yee (2002) and Yee and Sjögreen (2002) for the behavior of D06 and D08 central schemes with or without the AD8 and AD10 terms for longer time integration of this vortex convection problem. For a stable and accurate long time integration of periods up to 300, the central base scheme needs to be applied to the entropy split form of the inviscid flux derivative (instead of the conservative flux derivative). Similar long time integration of the vortex can also be obtained if our high order filter schemes are used. See Yee and Sjögreen (2000, 2002) for details.

In the second example we solve the 3-D Euler equations of gas dynamics with $\gamma = 5/3$ and with initial data

$$\rho(0,x,y,z) = 1 \tag{5}$$

$$u(0,x,y,z) = \sin(x)\cos(y)\cos(z) \tag{6}$$

$$v(0,x,y,z) = -\cos(x)\sin(y)\cos(z) \tag{7}$$

$$w(0,x,y,z) = 0 \tag{8}$$

$$p(0,x,y,z) = 100 + \frac{1}{16}((\cos(2z)+2)(\cos(2x)+\cos(2y)) - 2) \tag{9}$$

on the computational domain $[0, 2\pi] \times [0, 2\pi] \times [0, 2\pi]$. Here u, v, w are the three velocity components. This is known as a Taylor-Green vortex. The computation stops at a total time equal to 10. The boundary conditions are periodic.

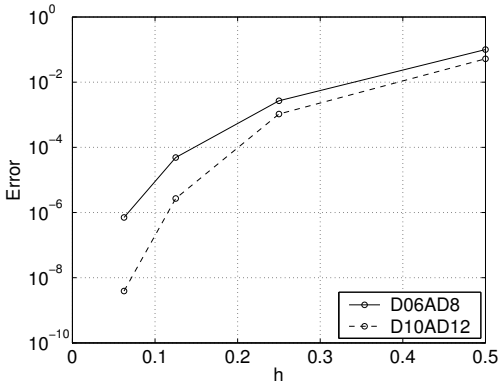

Figure 1: L^2 norm of the error in the density after the vortex has convected one period as function of the grid spacing, h. Sixth-order method (solid) and tenth-order method (dash).

The initial data are smooth, but the scales in the solution become smaller and smaller with time. The enstrophy (the square of the L^2 norm of the curl of the velocity) is often used as a measure of the content of small scales in the solution. For this problem, the added numerical dissipations AD8, AD10 and AD12, for the corresponding centered schemes are necessary for a stable time stepping.

In Fig. 2 we plot the enstrophy (normalized to 1 at time 0) as function of time for the sixth-order (dot), the eighth-order (dash) and the tenth-order (dash-dot) schemes, computed on a $64 \times 64 \times 64$ grid. We also plot the enstrophy obtained from the semi-analytical formulas given in Brachet et al. (1983). This "exact" solution is valid for times less than approximately 4 and we only plot it up to that time. The computed enstrophies agree well with the semi-analytical formula. The AD10 and AD12 numerical dissipation coefficients used are 0.00005. The D06AD8 with numerical dissipation coefficient 0.0001 is already unstable. The AD8 numerical dissipation coefficient used is 0.0002.

Figure 3 shows the same comparison as in Fig. 2, but with a $132 \times 132 \times 132$ grid using numerical dissipation coefficient of 0.0002 for AD8, 0.00006 for AD10 and 0.00002 for AD12. The maximum enstrophy now is higher (note different scaling) for all methods, reflecting the fact that higher frequencies can be supported on a finer grid. For this fine grid, the numerical dissipation coefficients 0.0001 for AD8, 0.00005 for AD10, and 0.00001 for AD12 give divergent solutions during the time evolution. Figure 4 shows the effect of the AD12 coefficient on the accuracy of the enstrophies of the tenth-order scheme using three different AD12 values (0.00005, 0.00003, and 0.00002).

The same computations using comparable yet larger dissipation coefficients for AD8, AD10 and AD12 are shown in Fig. 5 and Fig. 6 using 64^3 and 128^3 grid points. That is the strengths of the numerical dissipation operators are set to be equivalent for all three methods. The solution of the tenth-order scheme appears to follow the semi-analytical solution a bit closer. For large times there is no accuracy, but Fig. 5 shows that the schemes with less numerical dissipation give higher enstrophy values. Computations using central schemes with order lower than six give much lower enstrophy values (figures not shown) using the same two grids. This means that the method with the highest order of accuracy has the largest small-scale content. It is clear from Figs. 5 and 6 that the tenth-order method is better at supporting the small scales, because the enstrophy is higher for large times. In this case, the tenth-order central scheme is

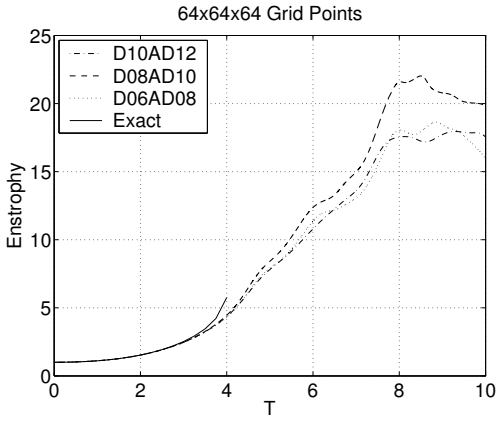

Figure 2: Enstrophy vs. time for the Talyor-Green vortex. 64^3 grid points. Sixth-order method with AD8 coeff. = 0.0002 (dot), eighth-order method with AD10 coeff. = 0.00005 (dash), tenth-order method with AD12 coeff. = 0.00005 (dash-dot), and semi-analytical (solid).

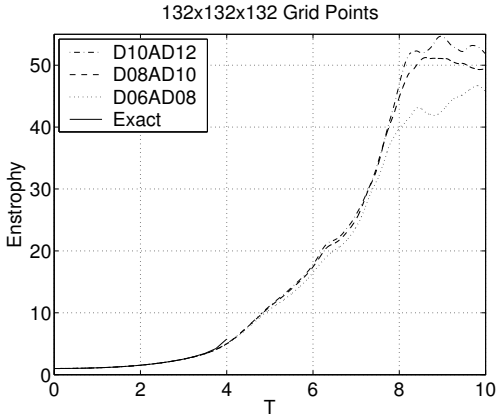

Figure 3: Enstrophy vs. time for the Talyor-Green vortex. 132^3 grid points. Sixth-order method with AD8 coeff. = 0.0002 (dot), eighth-order method with AD10 coeff. = 0.00006 (dash), tenth-order method with AD12 coeff. = 0.00002 (dash-dot), and semi-analytical (solid).

more accurate than its eighth-order and sixth-order counterparts. The above figures show the strong dependence of the ensthrophies on the gird size and the amount of their corresponding numerical dissipation coefficients of each methods. It is noted that if our high order filter schemes were used for this problem, for the same grid, lower enstrophy value were encountered due to the fact that shock-capturing dissipations are not needed here.

Both the above examples show error reduction with the tenth-order accurate scheme for problems with periodic boundary conditions. In order to extend the tenth-order computations to problems with non-periodic boundaries, special stable boundary operators are needed. We are particularly interested in deriving energy-norm stable SBP boundary operators for the tenth-order interior operator. One such derivation is presented next.

SBP DIFFERENCE OPERATORS

Here, we follow Strand (1994) to determine boundary modification for tenth-order accurate interior approximations of d/dx. We consider a uniform grid x_j, $j = 1, 2, 3, \ldots$

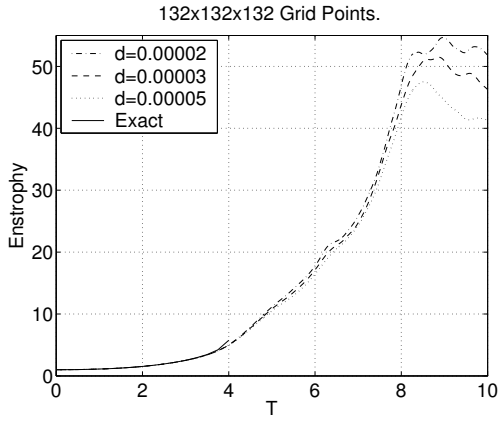

Figure 4: Enstrophy vs. time for the Taylor-Green vortex. 132^3 gird points. Tenth-order method with AD12 coeff. = 0.00002 (dash-dot), AD12 coeff. = 0.00003 (dash), AD12 coeff. = 0.00005 (dot), and semi-analytical (solid).

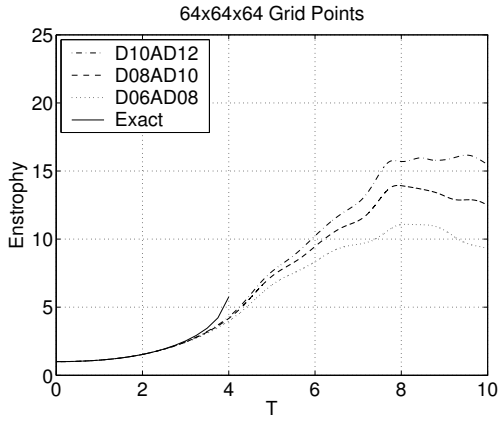

Figure 5: Enstrophy vs. time for the Talyor-Green vortex. 64^3 grid points using relative dissipation coefficient strength. Sixth-order method with AD8 coeff. = 0.0016 (dot), eighth-order method with AD10 coeff. = 0.0004 (dash), tenth-order method with AD12 coeff. = 0.0001 (dash-dot), and semi-analytical (solid).

with grid spacing $h = x_{j+1} - x_j$. The difference operator approximating $du(x_j)/dx$ is of the form

$$h\tilde{D}u_j = \begin{cases} \sum_{k=1}^{s} q_{j,k} u_k & j = 1, 2, \ldots, r \\ \sum_{k=-q}^{q} \alpha_k u_{j+k} & j = r+1, r+2, \ldots \end{cases}.$$

The interior approximation is defined by the coefficients α_k. The $2q$th order accurate interior approximation has $\alpha_{-k} = -\alpha_k$ and is used for $j > r$, where r is an arbitrary number $> q$. The boundary modified operator acts at the points $j = 1, \ldots, r$, and is defined by the coefficients $q_{j,k}$. The SBP boundary operator, which is the discrete analogue of the integration-by-parts energy norm, satisfy the identity

$$(u, \tilde{D}v)_h = -(\tilde{D}u, v)_h - u_1 v_1$$

for all grid functions u and v where $(u, v)_h$ is a discrete scalar product. This makes it possible to prove L^2-norm energy estimates for the difference approximation.

We write the difference operator in block matrix form as

$$h\tilde{D} = \begin{pmatrix} Q_1 & Q_2 \\ -C^T & D \end{pmatrix},$$

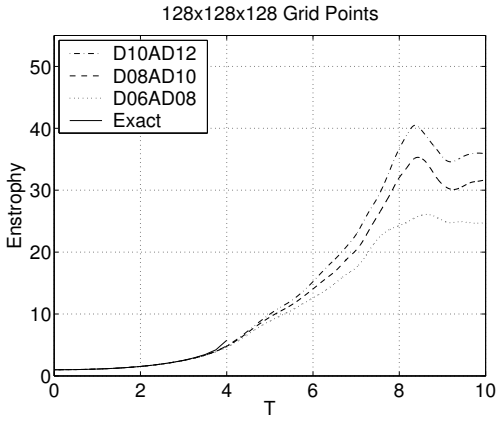

Figure 6: Enstrophy vs. time for the Talyor-Green vortex. 64^3 grid points using relative dissipation coefficient strength. Sixth-order method with AD8 coeff. = 0.0016 (dot), eighth-order method with AD10 coeff. = 0.0004 (dash), tenth-order method with AD12 coeff. = 0.0001 (dash-dot), and semi-analytical (solid).

where $Q = (Q_1\ Q_2)$ is the matrix formed by the coefficients $q_{j,k}$. Q_1 is of size $r \times r$. C and D are determined by the interior discretization. When the order of accuracy is $2q$, D is an anti-symmetric band matrix with constant diagonals

$$(-\alpha_q, -\alpha_{q-1}, \ldots, -\alpha_1, 0, \alpha_1, \ldots, \alpha_q),$$

where the zero is the main diagonal. The matrix C holds the part of the interior discretization that extends outside the first rows of D, i.e.,

$$-C^T = \begin{pmatrix} 0 & \ldots & 0 & -\alpha_q & -\alpha_{q-1} & \ldots & -\alpha_1 \\ 0 & \ldots & 0 & 0 & -\alpha_q & \ldots & -\alpha_2 \\ \ldots & \ldots & \ldots & \ldots & \ldots & \ldots & \ldots \\ 0 & \ldots & 0 & 0 & 0 & \ldots & -\alpha_q \\ 0 & \ldots & 0 & 0 & 0 & \ldots & 0 \\ \ldots & \ldots & \ldots & \ldots & \ldots & \ldots & \ldots \end{pmatrix}$$

Q_2 and C are of size $r \times (s - r)$. s can be considered arbitrarily large with the rows of Q_2 and C padded with zeros.

Taylor expansion gives the equations for pth-order of accuracy at the boundary,

$$QE = F \tag{10}$$

where $(E)_{i,j} = (i-1)^{j-1}$ and $(F)_{i,j} = (j-1)(i-1)^{j-2}$ and where any occurrence of 0^0 is interpreted as 1. The sizes of E and F are $s \times (p+1)$ and $r \times (p+1)$ respectively. We partition E as $E = \begin{pmatrix} E_1 \\ E_2 \end{pmatrix}$ with E_1 of size $r \times (p+1)$ and write (10) as

$$Q_1 E_1 + Q_2 E_2 = F. \tag{11}$$

The summation-by-parts property is equivalent to

$$(u, \tilde{D}u)_H = -\frac{1}{2}u_1^2$$

where the weighted scalar product is given by $(u, v)_H = (u^I)^T H v^I + (u^{II})^T v^{II}$, for a positive definite $r \times r$ matrix H. We define $u^I = (u_1, \ldots, u_r)$ and $u^{II} = (u_{r+1}, u_{r+2}, \ldots)$. The summation by parts property is equivalent to

$$HQ_1 = B_1 + B_2 \tag{12}$$

$$HQ_2 = C \tag{13}$$

where B_1 is the matrix with $-1/2$ as the (1,1) element and all other elements equal to zero. B_2 is an arbitrary anti-symmetric matrix. Consequently, the summation-by-parts boundary operators are found by solving (11), (12), and (13) for Q_1, Q_2, and H.

To solve these equations, we multiply (11) by H and use (12) and (13) to substitute HQ_1 and HQ_2. This results in the equation

$$B_2 E_1 + B_1 E_1 + C E_2 = HF \tag{14}$$

for B_2. We multiply (14) by E_1^T and use the anti-symmetry $(E_1^T B_2 E_1)^T = -E_1^T B_2 E_1$ to obtain the solvability condition

$$F^T H E_1 + E_1^T H F = 2E_1^T B_1 E_1 + E_1^T C E_2 + E_2^T C^T E_1 \triangleq M, \tag{15}$$

which is a linear system of $(p+1)^2$ equations for the r^2 unknown elements of H. We also require that H is symmetric. Note that M only depends on the interior discretization and on r. It was shown in Strand (1994) that (15) can be solved in the following cases

- p is odd, the interior discretization is $(p+1)$th-order accurate, and $r = p+1$, i.e., the number of equations and unknowns are equal in (15). H is called a full norm.
- p is odd, the interior discretization is $(p+1)$th-order accurate, $r = p+2$, and all elements on the first row of H, except the (1,1) element, are equal to zero. H is called a restricted full norm.
- H is diagonal, the interior discretization is $(2p)$th-order accurate, and $r = 2p$. H is called a diagonal norm.

Note that the existence of a solution H is not enough; in order for H to be a norm, H has to be positive definite as well. It was shown in Strand (1994) that a positive definite H can be found if r is made sufficiently large, but there is no guarantee that optimal properties $r = p+1$, $r = p+2$, and $r = 2p$ (for the three above cases) can be satisfied with H positive definite.

Energy estimates for PDEs obtained in one space dimension with the full norm operator do not generalize to two space dimensions, because the full norms in the x- and y-directions do not, in general, commute. With the diagonal norm, these operators do commute and estimates can be carried over from one dimensional problems to multidimensional problems. However, our experience from practical computations is that the full norm operators also perform well in multi-dimensions.

After having solved (15) for H, we insert H into (14) and solve for B_2. (14) is usually underdetermined and we obtain a solution that depends on a number of parameters. With H and B_2 known, (12) and (13) give $Q_1 = H^{-1}(B_1 + B_2)$ and $Q_2 = H^{-1}C$. The SBP boundary operator is determined. Table 1 summarizes a few known SBP operators. The second column shows the boundary order p and the third column displays the number of free parameters in the operator.

Olsson (1992) derived the same operators as Strand (1994). Mattson (2003) gave one operator, not the parametric dependency.

The freedom given by the undetermined parameters can be used, e.g., to determine an operator with a minimal spectral radius. This maximizes the time step if the operator is used in an explicit time stepping scheme.

Table 1: Summary of known SBP operators.

Norm type	B-order p	# param.	Ref.
full	3	2	Strand (1994)
full	5	3	Mattson (2003)
full	7	4	Mattson (2003)
restricted	3	3	Strand (1994)
diagonal	1	0	Strand (1994)
diagonal	2	0	Strand (1994)
diagonal	3	1	Strand (1994)
diagonal	4	3	Strand (1994)

SBP Operators with Tenth-Order Accuracy in the Interior

The tenth-order accurate centered finite difference operator has the coefficients

$$\alpha_1 = 5/6 \quad \alpha_2 = -5/21 \quad \alpha_3 = 5/84 \quad \alpha_4 = -5/504 \quad \alpha_5 = 1/1260. \quad (16)$$

We use this as the interior discretization and solve (15) for a diagonal norm with $p = 5, r = 10$. It turns out that the solution has negative elements, i.e., H is not positive definite. Similarly, solving for a diagonal norm SBP operator with $(p = 6, r = 12)$, $(p = 7, r = 14)$, and $(p = 8, r = 16)$ all give non-positive definite Hs. We conjecture that there are no diagonal norms as defined in Strand (1994) for $p > 4$.

Instead we take $p = 5$ and $r = 11$ to obtain an H that depends on one parameter. For a certain interval of the parameter, H is positive definite. We fix this parameter in the middle of the interval of positive definiteness to obtain the norm

$$H = diag(62715991/217728000,\ 10645069/6773760,\ 922613/6350400,\ 11862631/6350400,\ 678527/1036800,\ 21626453/36288000,\ 2887/1620,\ 678527/1814400,\ 130522139/101606400,\ 282939397/304819200,\ 64002913/63504000). \quad (17)$$

The SBP boundary operator, Q, thus obtained depends on 10 free parameters through the solution of (14). Setting random values of these parameters typically leads to an operator with a spectral radius of size 10^5, which is useless for any practical purpose. To overcome this problem, we used the `fminsearch` routine in Matlab to minimize the spectral radius of the difference operator with respect to the free parameters. The boundary operator obtained is presented in the Appendix. It has spectral radius 50, which is 20 times larger than the size of the interior operator, but it is small enough to enable some preliminary computations. The minimization problem is extremely ill-conditioned, and we have probably not reached the global minimum. This is a topic of continued investigation.

TEST CASE WITH NON-PERIODIC BOUNDARIES

The non-periodic test case is the 1-D compressible inviscid shock-turbulence interaction problem with initial data consisting of a shock propagating into an oscillatory density. The initial data is given by

$$(\rho_L,\ u_L,\ p_L) = (3.857143,\ 2.629369,\ 10.33333) \quad (18)$$

to the left of a shock located at $x = -4$, and

$$(\rho_R,\ u_R,\ p_R) = (1 + 0.2\sin(5x),\ 0,\ 1) \quad (19)$$

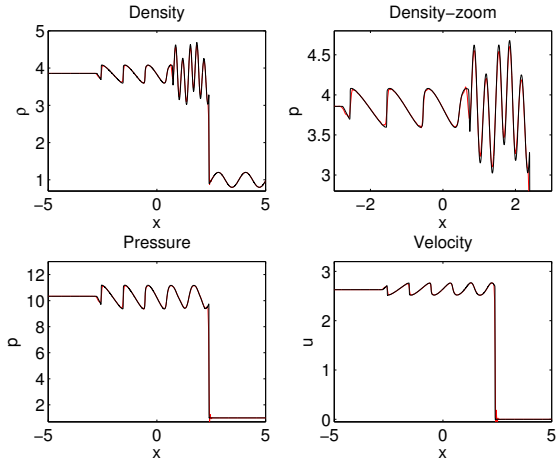

Figure 7: One dimensional shock-turbulence problem. Solution at time 1.6 computed by the new tenth-order SBP scheme with a fifth-order WENO based nonlinear filter (Yee and Sjögreen (2006)). Computed solution (grey) and reference solution (black).

to the right of the shock. The problem is solved on the domain $[0, 5]$.

Figure 7 shows the solution computed with the present SBP tenth-order spatial base scheme together with a nonlinear shock-capturing filter obtained as the dissipative portion of a fifth-order WENO scheme (Yee and Sjögreen, 1999, 2002, 2006). The computation used a uniform grid with 400 points (grey line) and the numerical dissipation coefficient of 0.0005 for AD12. The solid black line is the reference solution by the standard fifth-order WENO scheme using 4000 grid points. The SBP tenth-order filter scheme is very close to the reference solution. There is a dramatic improvement by the SBP tenth-order filter scheme over the standard fifth-order WENO scheme using the same grid (Yee and Sjögreen (2006, 2007)). Unfortunately, the accuracy of the SBP tenth-order filter scheme is almost indistinguishable from the SBP sixth-order and SBP eighth-order filter schemes computations for this particular test case. In addition, one major shortcoming of the SBP tenth-order scheme is that it has a very restricted CFL limit. It is an order of magnitude lower than its SBP sixth-order and SBP eighth-order counterparts. Note that the stable numerical boundary treatment (not SBP boundary operators) presented in Sjögreen (1995) is used for the dissipative difference operators AD8, AD10 and AD12 for the non-periodic boundary case. The SBP boundary operators for high order dissipative difference operators are very complicated. The present SBP boundary operator for the tenth-order central interior scheme is also used to simulate selected 2-D and 3-D multiscale problems containing strong shock waves. Results indicated that there is no dramatic gain in accuracy among sixth-order, eighth-order and tenth-order central base scheme under the framework of our high order filter approach. Perhaps an improved numerical boundary treatment for the AD12 difference operator and an improved filter strategy is needed to take advantage of the higher order accuracy base scheme for this type of multiscale physics. Future work includes the performance of the SBP tenth-order filter scheme for 3-D multiscale flows without shocks and for weak and strong shock/turbulence interactions with non-periodic physical boundaries. The results will be reported in detail in a future publication.

SUMMARY

We have presented a fifth-order SBP boundary modification for the tenth-order interior central scheme. However, increasing the interior accuracy higher than eighth-order in the derivation of SBP operators leads to new difficulties. First, it is non-trivial to make the norm matrices computed by the standard procedures positive definite. Second, the computed boundary operators usually have very large spectral radii. In the very high order case, both the norm matrices and the boundary operators depend on a large number of free parameters. In order to derive useful very high order SBP operators, it is necessary to use advanced optimization methods to select these parameters. For coarse grids with periodic boundary conditions, the tenth-order central differencing is more accurate than lower order schemes. For the non-periodic boundary case, the present SBP tenth-order scheme also performs well under the framework of our filter approach. However, the CFL limit of the tenth-order scheme is an order of magnitude lower than the sixth-order and eighth-order counterparts. Future work will include the study of SBP spatial compact interior schemes of order higher than four. The theory of SBP boundary modification for compact difference operators is not as complete as the theory for non-compact (central) operators. The method described in Carpenter et al. (1993) is specific to fourth-order accuracy only.

REFERENCES

Brachet, M.E., Meiron, D.I., Orszag, S.A., Nickel, B.G., and Morf, R.H., 1983, "Small-Scale Structure of the Taylor-Green Vortex", *J. Fluid Mech.*, Vol. 130, pp. 411–452.

Carpenter, M.H., Gottlieb, D., and Abarbanel, S., 1993, "The Stability of Numerical Boundary Treatments for Compact High-Order Finite-Difference Schemes," *J. comput. Phys.*, Vol. 108, pp. 272-295.

Kriess, H.-O. and Scherer, G., 1974, "Finite Element and Finite Difference Methods for Hyperbolic Partial Differential Equations", *Partial Differential Equations*, Academic Press, Inc.

Kriess, H.-O. and Scherer, G., 1977, "On the Existence of Energy Estimates for Difference Approximations for Hyperbolic Systems", Technical Report, Department of Scientific Computing, Uppsala University.

Mattson, K., 2003, "Summation-by-Parts Operators for High Order Finite Difference Methods", Ph.D. Thesis, Uppsala University, Information Technology, Department of Scientific Computing.

Olsson, P., 1992, "High-Order Difference Methods and Dataparallel Implementation" Ph.D. Thesis, Uppsala University, Department of Scientific Computing.

Olsson, P., 1995, "Summation by Parts, Projections, and Stability. I", *Math. Comp.*, Vol. 64, pp. 1035–1065.

Strand, B., 1994, "Summation by Parts for Finite Difference Approximations for d/dx", *J. Comput. Phys.*, Vol. 110, pp. 47–67.

Sjögreen, B., 1995, "High Order Centered Difference Methods for the Compressible Navier-Stokes Equations," *J. Comput. Phys.*, Vol. 117, pp. 67–78.

Sjögreen, B., and Yee, H.C., 2002, "Analysis of High Order Difference Methods for Multiscale Complex Compressible Flow", In *Proceedings of the HYP2002 conference*, Pasadena, CA, March 25-29.

Sjögreen, B., and Yee, H.C., 2003, "Grid Convergence of High Order Methods for Multiscale Complex Unsteady Viscous Compressible Flows", *J. Comput. Phys.*, Vol. 185, pp. 1–26.

Sjögreen, B., and Yee, H.C., 2004, "Multiresolution Wavelet Based Adaptive Numerical Dissipation Control for Shock-Turbulence Computation", *J. Sci. Comp.*, Vol. 20, pp. 211–255.

Yee, H.C., Sandham, N.D., Djomehri, M.J., 1999, "Low Dissipative High Order Shock-Capturing Methods Using Characteristic-Based Filters", *J. Comput. Phys.*, Vol. 110, pp. 47–67.

Yee, H.C., Vinokur, M., Djomehri, M.J., 2000, "Entropy Splitting and Numerical Dissipation," *J. Comput. Phys.* Vol. 162, pp. 33-81.

Yee, H.C., and Sjögreen, B., 2002, "Designing Adaptive Low Dissipative High Order Schemes for Long-Time Integrations", In *Turbulent Flow Computation*, Drikakis, D., and Geurts, B., ed., Kluwer Academic Publisher.

Yee, H.C., and Sjögreen, B., 2006, "Nonlinear Filtering and Limiting in High Order Methods for Ideal and Non-ideal MHD", *J. Sci. Comp.*, Vol. 27, pp. 507–521.

Yee, H.C., and Sjögreen, B., 2006, "Efficient Low Dissipative High Order Scheme for Multiscale MHD Flows, II: Minimization of Div(B) Numerical Error", RIACS Technical Report TR03.10, July, 2003, NASA Ames Research Center; also, J. Scient. Computing, (2005) DOI: 10.1007/s10915-005-9004-5, Vol. 29, pp. 115-164.

Yee, H.C., and Sjögreen, B., 2007, "Development of Low Dissipative High Order Filter Schemes for Multiscale Navier-Stokes/MHD Systems", Proceedings of the CalSpace/UCR ASTRONUM Conference, Palm Springs, CA, March 27-30, 2006. Expanded version to appear in J. Comput. Physics, 2007, http://dx.doi.org/10.1016/j.jcp.2007.01.012.

APPENDIX

Here we give the optimized boundary operator matrix Q for the SBP diagonal norm operator for the tenth-order interior scheme with $p = 5$ and $r = 11$. The matrix has size 11×16. The first six columns are

−1.735825	0.770205	5.598258	−5.303959	−5.536114	8.779473
−0.141173	0.000000	−2.878976	4.617511	1.976732	−5.979838
−11.099373	31.141411	0.000000	−66.660594	24.507405	76.519010
0.817870	−3.884603	5.184510	0.000000	−4.617298	−2.222004
2.436671	−4.746727	−5.440561	13.179402	0.000000	3.250455
−4.243363	15.768336	−18.653725	6.964703	−3.569390	0.000000
0.032496	−0.934761	4.439107	−8.991291	9.017526	−4.486641
0.665259	−3.113476	4.933463	−1.255448	−5.426069	7.335731
1.219606	−3.744699	−0.311858	13.619471	−18.761465	8.494855
−1.663525	5.798644	−2.675419	−13.658515	22.817263	−11.670627
0.408393	−1.510655	1.024657	2.833466	−5.397210	2.924868

columns seven to 11 are

−0.201045	−0.863696	−5.438996	5.360636	−1.428936
1.060019	0.740902	3.060986	−3.424987	0.968825
−54.451379	−12.698941	2.757407	17.093239	−7.108185
8.577760	0.251335	−9.365768	6.786950	−1.528751
−24.555401	3.100611	36.826269	−32.362533	8.311814
13.416241	−4.603151	−18.310359	18.177034	−4.946326
0.000000	0.908621	0.088411	−0.060118	−0.013795
−4.329925	0.000000	1.909337	−0.954379	0.259912
−0.122652	−0.555845	0.000000	−0.049806	0.173160
0.115421	0.384507	0.068928	0.000000	0.685535
0.024392	−0.096441	−0.220705	−0.631367	0.000000

and columns 12 to 16 are

0.000000	0.000000	0.000000	0.000000	0.000000
0.000000	0.000000	0.000000	0.000000	0.000000
0.000000	0.000000	0.000000	0.000000	0.000000
0.000000	0.000000	0.000000	0.000000	0.000000
0.000000	0.000000	0.000000	0.000000	0.000000
0.000000	0.000000	0.000000	0.000000	0.000000
0.000445	0.000000	0.000000	0.000000	0.000000
−0.026528	0.002122	0.000000	0.000000	0.000000
0.046337	−0.007723	0.000618	0.000000	0.000000
−0.256507	0.064127	−0.010688	0.000855	0.000000
0.826837	−0.236239	0.059060	−0.009843	0.000787